The 12th International Symposium on Transport Phenomena and Dynamics of Rotating Machinery
Honolulu, Hawaii, February 17-22, 2008

ISROMAC12-2008-20078

INFLUENCE OF INLET BOUNDARY CONDITIONS IN THE PREDICTION OF ROTOR DYNAMIC FORCES AND MOMENTS FOR A HYDRAULIC TURBINE USING CFD

M. Karlsson, H. Nilsson, J-O. Aidanpää

Lic. Eng. (M.Sc) Martin Karlsson
Division of Computer Aided Design, Luleå University of Technology, S-97187 LULEÅ, Sweden
Phone:+46705641911 Fax: +46920491399
karmar@ltu.se

Assistant Professor (Ph.D) Håkan Nilsson
Division of Fluid Dynamics, Chalmers University of Technology, S-41296 Gothenburg, Sweden
Phone:+46317721414 Fax: +4631180976
hani@chalmers.se

Associate Professor (Ph.D) Jan-Olov Aidanpää
Division of Solid Mechanics, Luleå University of Technology, S-97187 LULEÅ, Sweden
Phone:+46920492531 Fax: +46920491399
joa@ltu.se

ABSTRACT

The rotordynamic behavior of a hydraulic turbine is influenced by fluid-rotor interactions at the turbine runner. In this paper computational fluid dynamics (CFD) is used to numerically predict the rotordynamical excitation forces due to the flow through a hydraulic turbine runner. The simulations are carried out for three different boundary conditions. One axi-symmetric inlet boundary condition, and two axi-periodic boundary conditions. The two latter are obtained from separate simulations of wicket gate and spiral casing flow. It is found that the inlet boundary condition significantly affects the rotordynamical forces and moments.

INTRODUCTION

Hydraulic forces in rotordynamical models for turbines and pumps have been discussed during several years. Early investigations by Iversen et.al. (1960), Agostinelli et.al (1960) and Csanady (1962) introduced models of hydraulic unbalance forces due to asymmetry of the flow channel geometry in centrifugal pumps. Hergt and Krieger (1969-70), Colding-Jorgensen (1980), Adkins et.al., (1985), Adkins et.al. (1988), Bolleter et.al., (1988) included rotor whirling to develop models of fluid-rotor interactions of the pump impeller. Recent observation in rotordynamical measurements of commercial hydropower units by Gustavsson and Aidanpää (2003) and Karlsson and Aidanpää (2006) indicates that the fluid dynamics of the flow through the turbine affects the rotordynamical behavior of the hydropower unit.

During the last ten years, Computational Fluid Dynamics (CFD) has been more common in research and development of hydraulic machinery. However, in the field of modelling hydraulic excitations in rotordynamical models, CFD is not yet a common tool. It is of certain interest to evaluate if CFD can be used to analyze fluid-rotor interactions and excitations in hydraulic machinery, for example vibration at part discharge, hydraulic unbalance, blade passage and system characteristics.

The scope of this paper is to investigate how different boundary conditions in a CFD-model of a hydropower turbine runner affect the global rotordynamical forces on the turbine runner. Since rotordynamical analysis normally is carried out for a small model during a long simulation time and CFD-models normally have large degree of freedoms, it is of certain interest to develop models that are computational efficient. The computational cost will be depended also of the boundary conditions; hence it is important to investigate the impact of different boundary conditions.

NOMENCLATURE

β_m	Blending coefficient
ε	Eddy-viscosity
k	Turbulent kinetic energy
U	Velocity

MODELLING AND SIMULATIONS

The OpenFOAM CFD tool

In the present work the OpenFOAM (www.openfoam.org) open source CFD tool is used for the simulations of the fluid flow through the Hölleforsen water turbine runner. The simpleFoam OpenFOAM application is used as a base, which is a steady-state solver for incompressible, turbulent flow of non-Newtonian fluids. It is a finite volume solver using the SIMPLE algorithm for pressure-velocity coupling. It has been validated for the flow in the Hölleforsen turbine by Nilsson (2006). New versions of the simpleFoam application has been developed in the present work, including Coriolis and centrifugal terms and unsteady RANS. All the computations use wall-function grids and turbulence is modelled using the standard k-ε turbulence model. The computations have been run in parallel on 12 CPU's on a Linux cluster, using the automatic decomposition methods in OpenFOAM. The version number used for the present computations is OpenFOAM 1.4.

The Cases

The present work presents three different computations. All the computations are made for the Hölleforsen Kaplan turbine model runner. The computational grid is obtained from earlier calculations by Nilsson and Davidsson (2003). The operating condition used for the present investigations corresponds to a 60% load, a head of 4.5m, a flow rate of 0.522m^3/s, and is close to the best efficiency for the system. Three different inlet boundary conditions are applied in order to study the occurrence of unsteady effects. The resulting lateral forces and moments are calculated at each time step by integration of the pressure at the turbine runner blades. Figures 1 and 2 show the hydraulic system and an overview of the computational domain.

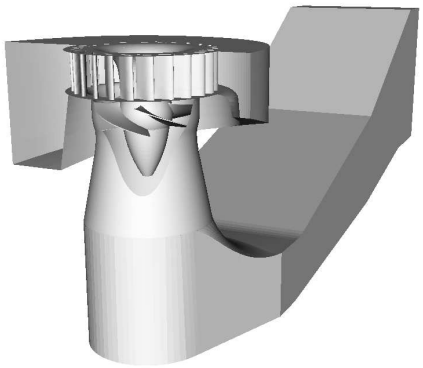

Figure 1. The geometry of Hölleforsen hydraulic system with the spiral casing, turbine runner and draft tube.

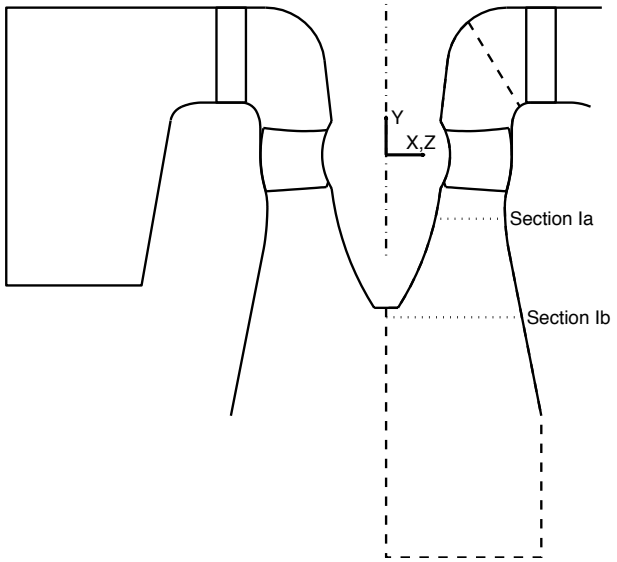

Figure 2. An overview of the part of the hydraulic system, used for the calculations. The dashed region in the right part of the figure is in the present work studied. Section 1a and 1b are used to compare simulations with measurement.

Boundary conditions

In order to investigate the influence of the non-axi-symmetry of the flow incident at the runner on the rotor dynamics, special inlet boundary conditions have been implemented in the present work. The first inlet boundary condition was obtained from a linear interpolation of the results from a separate wicket gate computation, presented by Nilsson and Davidsson (2003), yielding an axi-periodic boundary condition, see Figure 3. The runner is rotating with respect to the guide vanes and spiral casing, and the interpolated inlet boundary condition is thus counter-rotated with the runner rotational speed, yielding a rotating inlet boundary condition. This boundary condition is used for analyzing fluid-rotor interactions between the guide-vanes and the turbine runner.

The second inlet boundary condition was obtained by taking the circumferential average of the first boundary

condition, yielding in an axi-symmetric inlet flow, see Figure 4. This corresponds to a perfect distribution from the spiral casing and without any disturbance from the guide vanes.

The third inlet boundary condition was obtained using the result from a separate spiral casing computation by Oliveira de Souza and Nilsson (2002), yielding an axi-periodic boundary condition, see Figure 5. This boundary condition is used for analyzing fluid-rotor interactions due to the distribution from the spiral casing.

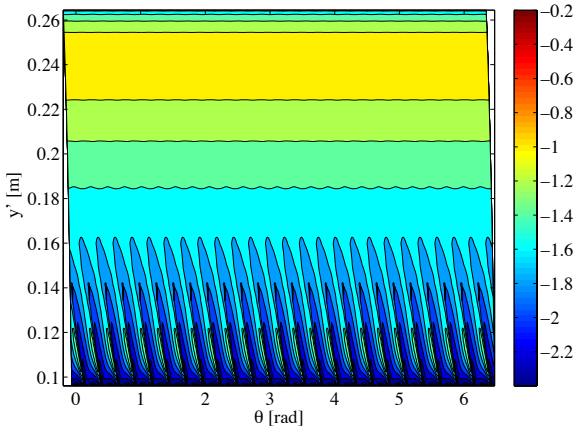

Figure 3. Inlet boundary condition (axial velocity component shown here) obtained from a separate wicket gate simulation. y' is the local coordinate at the inlet, parallel to y.

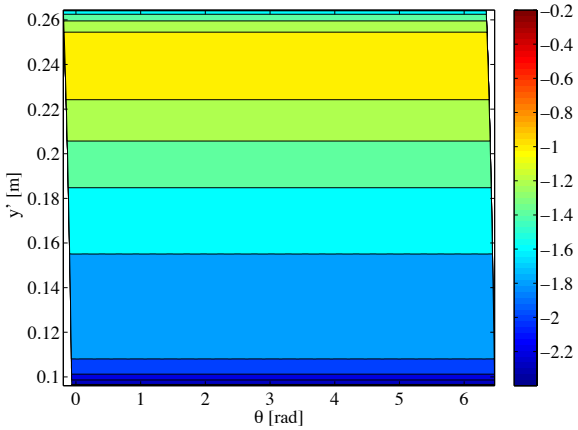

Figure 4. Inlet boundary condition (axial velocity component shown here) for the steady axi-symmetric flow. Y' is the local coordinate at the inlet, parallel to y.

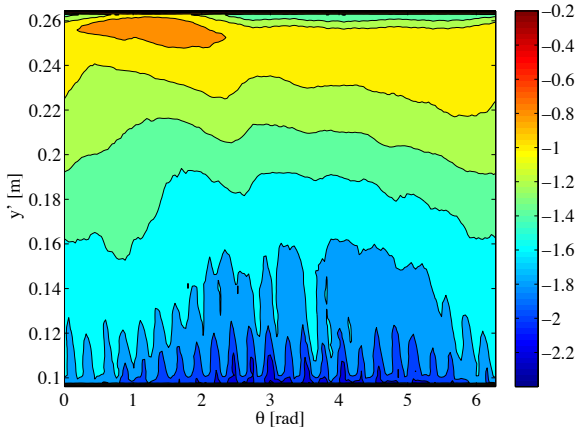

Figure 5. Inlet boundary condition (axial velocity component shown here) obtained from separate spiral case simulation. y' is the local coordinate at the inlet, parallel to y.

Wall-functions and rotating wall velocities were used at the walls, and at the outlet the homogeneous Neumann boundary condition was used for all quantities. Recirculating flow was thus allowed at the outlet. The turbulence quantities of the recirculating flow at the outlet are unknown, but to set a relevant turbulence level for the present case the back-flow values for k and ε were assumed to be similar to the average of those quantities at the inlet. The background of this assumption is that the turbulence level is high already at the inlet due to the wakes of the stay vanes, the guide vanes and the runner blades. It is thus assumed that the increase in turbulence level is small compared with that at the inlet. It is further believed that the chosen values are of minor importance to the overall flow. For the pressure the homogeneous Neumann boundary condition is used at all boundaries. The turbulence is modeled with the standard k-ε model.

Grid

The computations are made for a complete runner with five blades. A block-structured hexahedral wall-function grid was used, consisting of approximately 2, 200, 000 grid points.

Discretization schemes

For the convection divergence terms in the turbulence equations the Gamma discretization scheme by Jasak et.al. (1999) was used. For the convection divergence terms in the velocity equations the GammaV scheme was used, which is an improved version of the Gamma scheme formulated to take into account the direction of the flow field. The Gamma scheme is a smooth and bounded blend between the second-order central differencing (CD) scheme and the first order upwind differencing (UD) scheme. CD is used wherever it satisfies the boundedness requirements, and wherever CD is unbounded UD is used.

For numerical stability reasons, however, a smooth and continous blending between CD and UD is used as CD approaches unboundedness. The smooth transition between the CD and UD schemes is controlled by a blending coefficient β_m, which is chosen by the user. This coefficient should have a value in the range $0.2 \leq \beta_m \leq 1$, the smaller value the sharper switch and the larger value the smoother switch between the schemes. For good resolution, this value should be kept as low as possible, while higher values are more numerically stable. In the present work a value of $\beta_m = 1.0$ has been used. The time derivate is discretized using the Euler implicit method.

RESULTS

In Figures 6 and 7 the calculated velocity coefficient distributions for each simulated case is compared with the measurements presented by Andersson (2000) for section 1a and 2b (see Figure 2).

In Figures 8, 11 and 15 the runner blade force in x-direction and in Figures 9, 12 and 16 the runner blade moments around the x-axis, are shown for the three different inlet boundary conditions. The forces are scaled with the force obtained from an unbalance of quality grade 6.3 according to ISO 1940. The moment is scaled with the nominal torque. In Figures 10, 14 and 17 the inlet velocity and a pressure iso-surface are shown. In Figure 13 the vortex is identified with the normalized helicity for the case with wicket gate inlet boundary condition. Figure 18 shows a comparison of the lateral forces for the different boundary conditions.

Forces and moments are filtered with a 9th order butterworth lowpass filter. In order to avoid numerical perturbations the cut off frequencies are selected separately for the three different cases; 50 times rotational speed for the case with inlet boundary condition based on separate wicket gate calculation, 25 times rotational speed for the case with axi-symmetric inlet boundary condition and 75 times rotational speed for the case with inlet boundary condition based on separate spiral casing calculation.

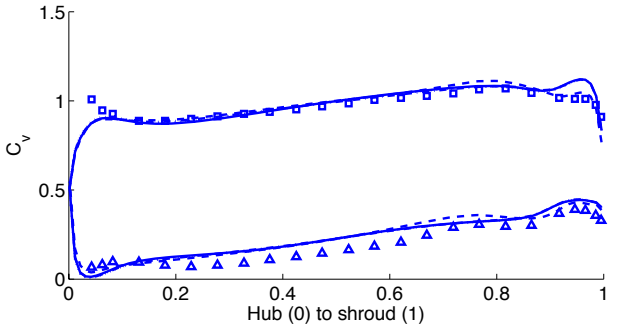

Figure 6. Comparison of axial and tangential coefficient of velocity at section 1a (see Figure 2). Dashed-dotted lines are for the wicket gate inlet boundary case, solid lines for the steady axi-symmetric inlet boundary case and dashed lines for the spiral casing inlet boundary case. Measured values are marked with squares (axial component) and triangles (tangential component). Note that the coeffcient of velocity is the same for the case with axi-symmetric boundary condition and boundary condition based on separate wicket gate calculation.

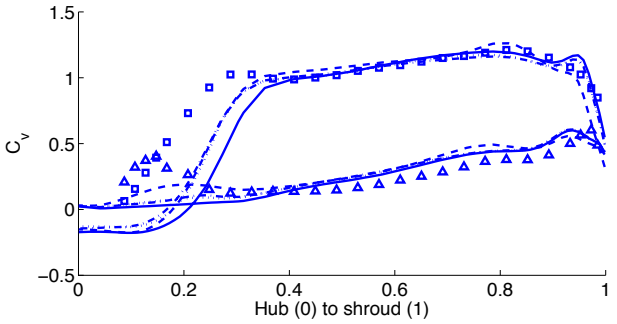

Figure 7. Comparison of axial and tangential coefficient of velocity at section 1b (see Figure 2). Dashed-dotted lines are for the wicket gate inlet boundary case, solid lines for the steady axi-symmetric inlet boundary case and dashed lines for the spiral casing inlet boundary case. Measured values are marked with squares (axial component) and triangles (tangential component).

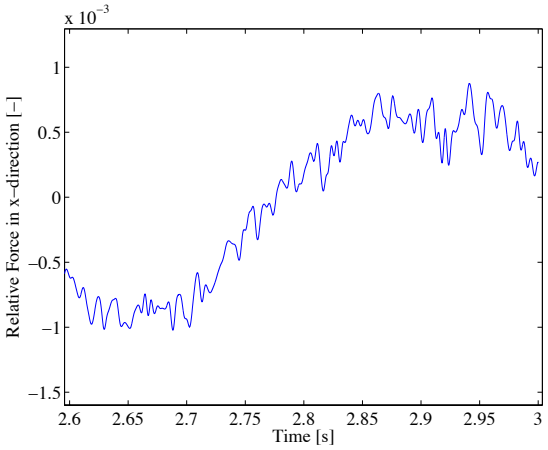

Figure 8. Lateral force at the turbine runner blades in the x-direction (inertial system) for the inlet based on steady and axi-symmetric boundary condition.

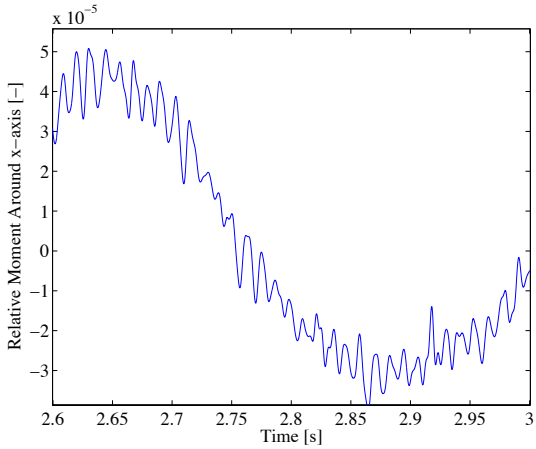

Figure 9. Lateral moment at the turbine runner blades around the x-axis (inertial system) for the inlet based on steady and axi-symmetric boundary condition.

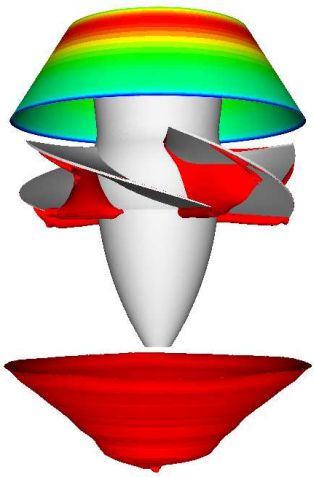

Figure 10. Axial velocity component at the rotating inlet and pressure iso-surface for the axi-periodic boundary condition based on wicket gate calculation. The non-axisymmetry in pressure shown in the figure is fluctuating.

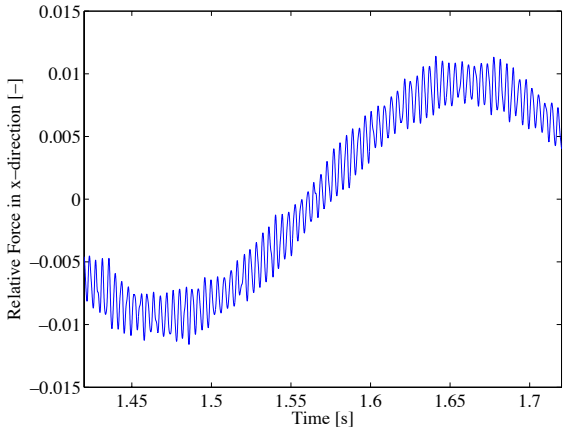

Figure 11. Lateral force at the turbine runner blades in the x-direction (inertial system) for the inlet boundary condition based on wicket gate wakes calculation.

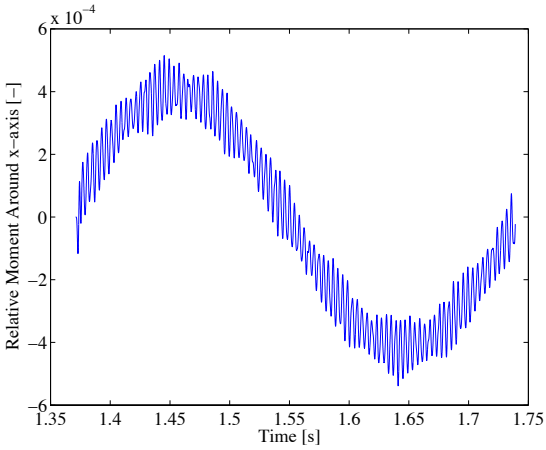

Figure 12. Lateral moment at the turbine runner blades around the x-axis (inertial system) for the inlet boundary condition based on wicket gate calculation.

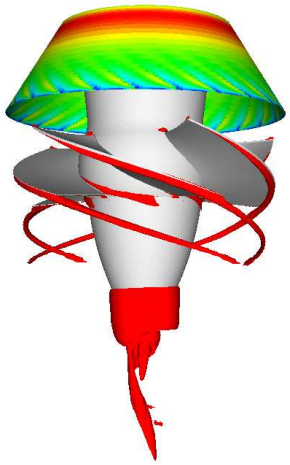

Figure 13. Axial velocity component at the rotating inlet and normalized helicity for visualization of the vortices.

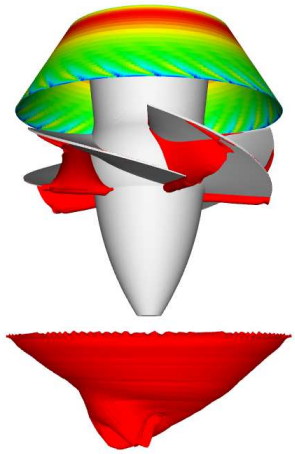

Figure 14. Axial velocity component at the rotating inlet and pressure iso-surface for the axi-periodic boundary condition based on wicket gate calculation. The non-axisymmetry in pressure shown in the figure is fluctuating.

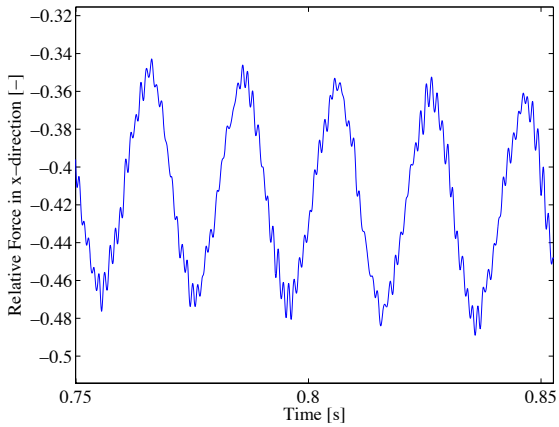

Figure 15. Lateral force at the turbine runner blades in the x-direction (inertial system) for the inlet boundary condition based on separate spiral casing calculation.

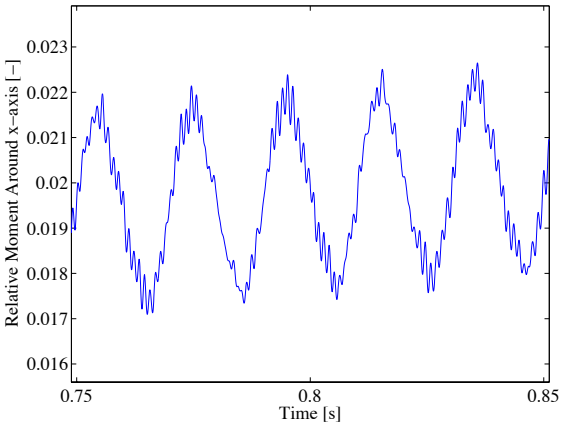

Figure 16. Lateral moment at the turbine runner blades around the x-axis (inertial system) for the inlet boundary condition based on separate spiral casing calculation.

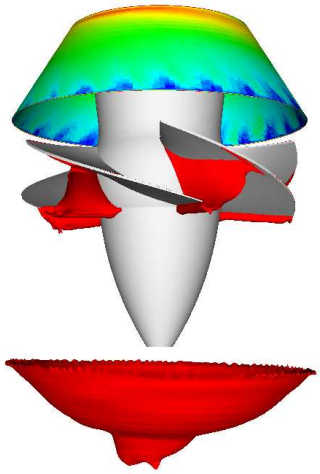

Figure 17. Axial velocity component at the rotating inlet and pressure iso-surface for the boundary condition based on the separate spiral casing calculation. The non-axisymmetry in pressure shown in the figure is fluctuating.

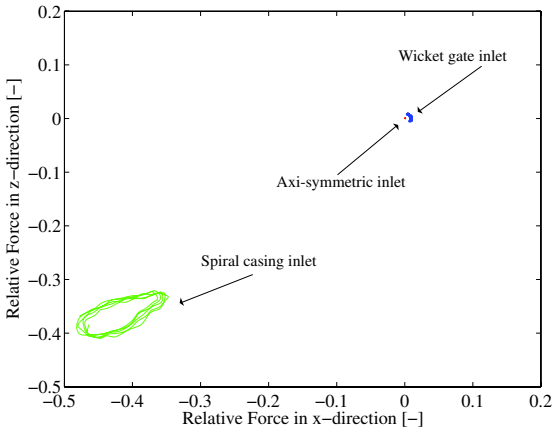

Figure 18. Comparison of the lateral force in x- and z-direction (inertial system) during one revolution for the three different inlet boundary conditions during one revolution. The large green orbit is the case using spiral casing inlet, the blue orbit is obtained from wicket gate inlet and the red dot is the axi-symmetric inlet.

DISCUSSION

Three different inlet boundary conditions have been used in the simulations of a hydropower turbine model, in order to calculate the resulting forces and moments on the runner blades. The amplitude of both the forces and moments are larger for the case with the inlet boundary condition obtained from the spiral casing calculation compared to the case with an inlet boundary condition based on axi-symmetric flow and separate wicket gate calculation. However, the amplitude of the forces are relative small, for example is the largest dynamic force about 6% and the largest static force about 35% of an unbalance force of quality grade G6.3. The simulations are carried out for an operation near best efficiency and one can expect that the excitation forces will increase for other operation conditions.

Figures 6-7 show comparisons between the velocity coefficients and the measurements at two cross-sections. The simulations show acceptable agreements with measurements for the main part of the sections. However, the calculated velocity coefficients do not agree with the measurements near the hub. A simplification of the geometry, which does not include the runner's hub clearance, is a possible explanation to the difference between measurement and simulations according to Nilsson (2006). One can also note that the case with an inlet boundary condition based on the separate spiral casing calculation better predicts some effects of the velocity coefficient near the shroud.

For all the cases a low frequency force is present. The frequency of this force is about 1/4 of the rotational speed and is possible an effect of a vortex rope below the runner. This effect is largest for the case based on separate spiral

casing calculation followed by the case based on separate wicket gate calculation. Hence, the use of non-axi symmetric inlet boundary conditions will lead to a non axi-symmetric flow downstream, which seems to trigger the initialisation of a vortex rope.

For the case with inlet boundary condition based on separate wicket gate calculation, a high frequency force (due to the wakes behind the wicket gate) is present. The same effect might be shown in the case based on separate spiral casing calculation, where small perturbations in the periodic force are present. However, the wakes are not distinguished shown as separate wakes at the inlet (see Figure 5). Hence it is not obvious that the force due to interaction with the wicket gates should be periodic with the same frequency as in the case with boundary based on separate wicket gate calculation. One could therefore suppose that the perturbations are an effect of the axi-periodic variation at the inlet. One probable reason to the comparably small forces due to the interactions with the wicket gate is the computational grid. The wake flow travels a long distance diagonally through relatively large computational cells. This has a dissipative effect on the wakes. For the case with inlet boundary condition based on the separate spiral casing calculation also a static force and force due to blade passage are present, which are effects of the asymmetric inlet flow.

The pressure fluctuations that are the source of the lateral forces do also result in bending moments, with the same frequencies as the forces. However, the dynamic moment for all simulation is less than 1% of torque. For the case with an inlet boundary condition based on separate spiral casing calculation is a static moment of about 2% of the torque present.

The model used for the CFD does not contain the upstream (penstock and spiral casing) and downstream (draft tube) fluid domains. Since the inlet boundary condition is affecting the results of the simulations, one future investigation can be to investigate how the upstream and downstream domains affect the flow through the turbine and affect the resulting forces and moments.

CONCLUSIONS

It has been found that there is a significant difference in resulting lateral forces and moments depending on which inlet boundary condition is applied to the CFD-model. The model with inlet boundary conditions obtained from the separate spiral casing calculation results in the largest hydraulic forces and moments on the turbine runner blades. These forces might excite the rotor system and it is therefore important to consider them during design of the whole rotor system, including bearings, generator and supporting structure.

ACKNOWLEDGEMENT

The research presented in this paper has been carried out with funding by Elforsk AB and the Swedish Energy Agency through their joint Elektra program and as a part of "Swedish Hydropower Centre - SVC" (www.svc.nu). SVC has been established by the Swedish Energy Agency, Elforsk and Svenska Kraftnät together with Luleå University of Technology, The Royal Institute of Technology, Chalmers University of Technology and Uppsala University. Computations have been carried out with support by Swedish National Infrastructure for Computing on the hive and ada clusters at C3SE, Chalmers University of Technology.

Mr. Eduardo Oliveira de Souza is gratefully acknowledged for sharing data from his earlier simulations of the spiral casing. The developers and community of OpenFOAM are gratefully acknowledged for sharing their code and for interesting discussions on the Internet forum and workshops.

REFERENCES

Adkins, D. R., Analysis of Hydrodynamic Forces on Centrifugal Pump Impellers, Ph.D. Thesis, California Institute of Technology, Pasadena CA, 1985

Adkins, D. R. and Brennen, C.E., 1988, Analyses of Hydrodynamic Radial Forces on Centrifugal Punp Impellers, ASME Journal of Fluid Engingeering, Vol. 110, pp20-28, 1988

Agostinelli, A., Nobles, D., and Mockridge, C. R., An Experimental Investigation of Radial Thrust in Centrifugals Pumps, ASME Journal of Engineering for Power, Vol. 82, pp.120-126.

Andersson, U., Turbine 99 - Experiments on draft tube flow (test case T), Proceedings from Turbine 99 - Workshop on Draft Tube Flow, 2000, ISSN: 1402 – 1536.

Bolleter, U,, Leibundgut, E., Struchler, R. and Closkey, T., Hydraulic Interaction and Excitation Forces of High Head Pump Impellers, Pumping Machinery – 1989, Vol 81, 3rd Joint ASCE/ASME Mechanics Conference, UCSD, July 9-12, 1989, pp. 187-193.

Colding-Jorgensen J., The Effect of Fluid Forces on Rotor Stability of Centrifugal Compressors and Pumps, First Workshop on Rotordynamic Instability Problems in High Performance Turbomachinery, Texas A&M University, NASA Conf. Pub. 2443, pp- 249-266, 1980

Csanady, G.T., Radial Forces in a Pump Caused by Volute Casing, ASME Journal of Engineering for Power, Vol. 84, pp. 337-340, 1962

GustavssonR. K. and Aidanpää J-O. Measurement of bearing load using strain gauges at hydropower unit.HRW.Vol 11, November 2003

Hergt, P. and Krieger, P., Radial Forces in Centrifugal Pumps With Guide Vanes, Proc. Inst. Mech. Eng., Vol. 184, Part 3N, pp. 101-107, 1969-70

Iversen, H. W., Rolling, R. E. and Carlson, J. J,, Volute Pressure Distribution, Radial Forces on the Impeller and Volute Mixing Losses of a Radial Flow Centrifugal Pump, ASME Journal of Engingeering for Power, Vol. 82, pp-136-44, 1960.

Jasak, H., Weller, H.G., Gosman, A.D., High Resolution NVD Differencing Scheme for Arbitrarily Unstructured Meshes, International Journal for Numerical Methods in Fluids, p.431—449, 1999.

Karlsson, M., Aidanpää, J-O., Characteristics of a Hydro Power Rotor System due to a Sudden Loss of Magnetic Field, 7th IFToMM-Conference on Rotor Dynamics, Vienna, Austria, 25-28 September 2006

Nilsson, H., Davidson, L., A Numerical Investigation of the Flow in the Wicket Gate and Runner of the Hölleforsen (Turbine-99) Kaplan Turbine Model. Proceedings of Turbine 99 – II, 2001

Nilsson, H., Davidson, L., Validations of CFD against detailed velocity and pressure measurements in water turbine runner flow, International Journal for Numerical Methods in Fluids, 41, p.863-879, 2003.

Nilsson, H., Evaluation of OpenFOAM for CFD of turbulent flow in water turbines. IAHR Symposium 2006, Yokohama.

Oliveira de Souza, L. C. E., Dias de Moura, M.; Brasil J., Antonio C.P. Nilsson, H., Assessment of turbulence modelling for CFD simulations into hydroturbines: spiral casings. 17th International Mechanical Engineering Congress (COBEM 2003) at São Paulo (Brazil)